Polymer Chemistry

Accepted Manuscript

This is an *Accepted Manuscript*, which has been through the Royal Society of Chemistry peer review process and has been accepted for publication.

Accepted Manuscripts are published online shortly after acceptance, before technical editing, formatting and proof reading. Using this free service, authors can make their results available to the community, in citable form, before we publish the edited article. We will replace this *Accepted Manuscript* with the edited and formatted *Advance Article* as soon as it is available.

You can find more information about *Accepted Manuscripts* in the Information for Authors.

Please note that technical editing may introduce minor changes to the text and/or graphics, which may alter content. The journal's standard Terms & Conditions and the Ethical guidelines still apply. In no event shall the Royal Society of Chemistry be held responsible for any errors or omissions in this *Accepted Manuscript* or any consequences arising from the use of any information it contains.

ROYAL SOCIETY OF CHEMISTRY

www.rsc.org/polymers

Polymer Chemistry

ARTICLE

Study of Thiol-Ene Chemistry on Polymer Brushes and Application to Surface Patterning and Protein Adsorption

Received 00th January 20xx,
Accepted 00th January 20xx

DOI: 10.1039/x0xx00000x

www.rsc.org/

Khooi Y. Tan,[a] Madeleine Ramstedt,[b] Burcu Colak,[c,d] Wilhelm T. S. Huck[e]† and Julien E. Gautrot[c,d]†

Polymer brushes are attractive polymeric coatings for biomedical applications such as tissue engineering, biosensor design and the purification of biological samples. In order to confer bioactivity to these coatings, their functionalisation with biomolecules, proteins and peptides, is required. In this respect, thiol-ene coupling offers interesting features as it is regioselective, efficient and can be controlled by photo-irradiation to allow surface patterning. The efficiency of thiol-ene and the related thiol-yne couplings to poly(glycidyl methacrylate) brushes was quantified. The impact of the structure of thiols to be tethered and reaction conditions on the brush loading and the kinetics of reaction were investigated. Thiol-ene reactions were then used to pattern brushes via direct irradiation through a mask or via reactive micro-contact printing. The resulting patterns were used to control albumin adsorption and the formation of protein patterns.

Introduction

The design of biointerfaces is an essential component of the development of biomedical applications such as biosensors, chromatography and purification platforms, as well as for cell culture and tissue engineering. The chemistry of such biointerfaces plays an important role in controlling biological properties such as bioinertness[1], specific binding and recognition of biomolecules and analytes[2], and the promotion of cell adhesion and proliferation[3]. Polymer brushes are particularly attractive coatings to achieve and tune such properties as their chemistry is compatible with a wide range of substrates without compromising bulk mechanics, morphology or the sensitivity of sensors[4]. Their chemistry can be tailored easily, through the vast library of monomers polymerisable via controlled polymerisation techniques, and their quasi-3D morphology offers interesting advantages to conventional self-assembled monolayers in terms of stability, amplification of surface chemistry, density of functional groups, diffusion barrier to moderately small molecules and ability to form highly solvated interfaces[5, 6]. Hence highly protein resistant polymer brushes have been successfully used to generate robust platforms for cell patterning and for the control of cell shape and phenotype[7-10]. Such cell-based arrays are attractive for systematic quantification of cell behaviour and the study of underlying molecular processes.

In many cases the use of polymer brushes for biomedical applications requires their bio-functionalisation[4, 11] in order to confer properties such as bio-recognition and cell adhesion. However the coupling of proteins and peptides to polymer brushes remains challenging, in particular in the case of anti-fouling polymer brushes. In this respect, successful strategies include traditional ester, amide, carbonate and urethane formation through coupling to repeat units activated using disuccinimidyl carbonate[12], N-(3-dimethylaminopropyl)-N-ethylcarbodiimide hydrochloride and N-hydroxysuccinimide (EDC/NHS)[13] or nitrophenyl chloroformate[14]. Thiol-maleimide coupling was also used to functionalise poly(ethylene glycol methacrylate) brushes with cysteine-terminated peptides[15]. Other successful approaches were based on biotin-streptavidin binding[12, 16] or the capture of histidine-tagged proteins by nickel nitrilotriacetate complexes[17, 18]. However, these strategies often do not result in the control of regioselectivity and the orientation of tethered biomolecules, or their patterning. In this respect, click reactions such as those based on copper-free azide-alkyne[19], Diels-Alder[20] and phototriggered nitrile imine-mediated tetrazole-ene cyclocloaddition reactions[21] offer advantages in terms of efficiency of coupling and selectivity. Thiol-ene chemistry is particularly attractive as it can efficiently couple otherwise unreactive alkenes (compared to maleimide and acrylates used in Michael type additions) to thiols, including cysteines[22, 23]. This reaction is very efficient, even in the presence of oxygen and is compatible with photo-patterning, when mediated by radical photoinitiators. Hence thiol-ene coupling has been

[a] Melville Laboratory for Polymer Synthesis, Department of Chemistry, University of Cambridge, Lensfield Road, Cambridge, CB2 1EW, UK.
[b] Department of Chemistry, Umeå University, SE-90187 Umeå, Sweden.
[c] Institute of Bioengineering, Queen Mary, University of London, Mile End Road, London, E1 4NS, UK.
[d] School of Engineering and Materials Science, Queen Mary, University of London, Mile End Road, London, E1 4NS, UK.
[e] Radboud University Nijmegen, Institute for Molecules and Materials, Heyendaalseweg 135, 6525 AJ Nijmegen, The Netherlands.
†Correspondence should be addressed to j.gautrot@qmul.ac.uk and w.huck@science.ru.nl.
Electronic Supplementary Information (ESI) available: details of calculation of functionalization ratios, additional ellipsometry, NMR, FTIR, XPS and water contact goniometry. See DOI: 10.1039/x0xx00000x

used previously to post-functionalise polymers[24-26], control the crosslinking of hydrogels[27-29], biofunctionalise materials[23, 29] and as a tool for photo-patterning self-assembled monolayers[30].

In addition, some reports have shown that thiol-ene and the related thiol-yne couplings are effective methods for the post-polymerisation functionalisation of polymer brushes[26, 31, 32]. We recently used this approach to couple cell adhesive peptides to otherwise protein and cell-resistant brushes, *in situ* after initial cell adhesion and spreading to unprotected micropatterned areas[33]. This platform was used as a novel type of model for wound healing assays and it was demonstrated that cell migration on such systems was dependent on peptide density. However the efficiency of thiol-ene coupling to polymer brushes has not been systematically studied. This study explores the efficiency of thiol-ene coupling to functionalise polyglycidyl methacrylate (PGMA) brushes, as a simple easily accessible model system (see Scheme 1). The impact of the chemical structure of the thiol and reaction conditions on coupling efficiency is quantified, to determine optimal reaction conditions and kinetics of coupling. The use of thiol-yne coupling for brush functionalisation is also investigated. Finally, thiol-ene coupling was used to photopattern PGMA brushes via direct photo-irradiation through a photomask and via reactive micro-contact printing. The resulting patterned brushes were then used to control the adsorption of bovine serum albumin and the generation of protein patterns.

Materials and methods

Chemicals and materials

Surface ATRP initiator, (3-trimethoxysilyl)propyl-2-bromo-2-methylpropionate **1**, was supplied by Gelest. Free ATRP initiator, poly(ethylene glycol) bromobutyrate **2** was synthesised according to a previous procedure[34]. Glycidyl methacrylate (GMA), poly(ethylene glycol) methyl ether methacrylate (average $M_n \approx 300$) (OEGMA), Cu(ii)Br_2, 2,2-dimethoxy-2-phenylacetophenone **P1**, 4,4'-bis(diethylamino)benzophenone **P2**, 2,4-diethyl-9*H*-thioxanthen-9-one **P3**, phenylbis(2,4,6-trimethylbenzoyl)phosphine oxide **P4**, cysteamine hydrochloride **T1**, *N*-acetyl L-cysteine **T2**, allylamine, propargylamine, thioglycolic acid **T3**, reduced l-glutathione **T4**, Cu(i)Cl, 2,2'-dipyridyl (bipy), bovine serum albumin (BSA) and 3-aminopropyltrimethoxysilane (APTMS) were purchased from Sigma-Aldrich. Triethylamine (Et_3N) was purchased from Alfa Aesar. Phosphate-buffered saline (PBS) pH 7.3 tablets were supplied by Oxoid. Methoxy poly(ethylene glycol) (PEG) thiol **T5** ($M_w \approx 356.5$ g/mol, purity >95%) was purchased from Polypure. CGGGRGDS peptide **T6** ($M_w \approx 706.72$, purity 80-95%) was supplied by Cambridge Peptides. Biotin PEG thiol **T7** ($M_w \approx$ 2000 g/mol) was supplied by Nanocs. Bovine serum albumin conjugated with Alexa Fluor® 555 dye (BSA-dye) was purchased from Life Technologies. Chemicals and reagent-grade solvents were used as received unless otherwise stated. Cu(i)Cl was kept under vacuum until needed. Et_3N was distilled from KOH and stored over molecular sieves (3 Å grade). Absolute ethanol was used. Purified water with a resistivity of 18.2 MΩ·cm was obtained from a Millipore Synergy system. Anhydrous toluene and *N*,*N*-dimethylformamide (DMF) were withdrawn from a PureSolv solvent purification system (Innovative Technology). Silicon wafers (diameter 100 mm, orientation ⟨100⟩, one side polished) were purchased from Compart Technology. Borosilicate glass cover slips (thickness no. 1) were obtained from Fisher Scientific. Silicon wafers and glass cover slips were cleaned in an air plasma with a forward power of 100 W (Emitech K1050X plasma asher) for 10 min before use. Polyester-based film photomasks were supplied by Micro Lithographic Services. PDMS stamps for micro-contact printing were prepared according to an established procedure[35] using a Sylgard® 184 silicone elastomer kit (Dow Corning) cast over a master generated from SU8 negative photoresist.

Generation of polymer brushes via surface-initiated ATRP

ATRP initiator or APTMS was coated on silicon wafers or glass cover slips via self-assembly according to a published procedure[36] using solutions containing ATRP initiator **1** or APTMS (10 µL), Et_3N (50 µL) and anhydrous toluene (50 mL). Following this, PGMA or POEGMA brushes were synthesised on silicon wafers or glass cover slips coated with ATRP initiator **1** following an established procedure[7, 37]. All steps were performed at room temperature (RT, ~20 °C). Formulations: for PGMA[37], GMA 15 mL (110 mmol), bipy 423 mg (2.7 mmol), Cu(ii)Br_2 11.7 mg (50 µmol), Cu(i)Cl 109.2 mg (1.1 mmol), methanol/water (4/1 v/v) 15 mL, each degassing 20 min, rinsed with methanol, tetrahydrofuran (THF) and ethanol after polymerisation; for POEGMA[7], OEGMA 6.3 g (17.5 mmol), bipy 160 mg (1.0 mmol), Cu(ii)Br_2 9 mg (40 µmol), Cu(i)Cl 41 mg (410 µmol), ethanol/water (4/1 v/v) 15 mL, each degassing 30 min, rinsed with water and ethanol after polymerisation.

Aminolysis of PGMA brushes

Addition of alkene or alkyne to PGMA was carried out according to a published procedure[38]. Substrates coated with PGMA brushes were immersed in DMF. An equal volume of a solution containing allylamine or propargylamine (4 M) and triethylamine (25 mol% with respect to allylamine or propargylamine) was added to the substrates and mixed thoroughly. Reaction was allowed to proceed at 40 °C for 24 h. The substrates were then rinsed with DMF and ethanol before drying under a stream of nitrogen gas.

Thiol-ene reaction *via* photolithography

A solution consisting of a thiol of interest and a photoinitiator in a solvent was deoxygenated via nitrogen gas bubbling for at least 15 min. A substrate (~1 × 1 cm^2) containing PGMA brushes functionalised with allylamine or propargylamine was assembled for photoinitiated thiol-ene/-yne reaction according to the set-up as illustrated in Figure S8 and exposed to UV at 365 nm (UV LED array, 672 LEDs, Cetoni GmbH) for a desired period. The substrate was removed, incubated in PBS for 15

min, rinsed thoroughly with DMF, water and ethanol before drying under a stream of nitrogen gas. Clear photomasks without prints were used for homogeneous functionalisation. Formulations: for homogeneous functionalisation, **T1-T6** 25 M, **P1**-**P4** 2.5 mM, DMF (**T1-T3**) or DMF/water 1/1 v/v (**T4-T6**), 15 min UV irradiation (DMF/water mixture was used as these thiols were insoluble in pure DMF); **T7** 5 mM, **P2** or **P4** 12 mM, DMF, 15 min UV irradiation; for kinetic studies as in Figures 3 and S6, **T1** 2.4 M, **P1**-**P4** 2 wt% with respect to **T1**, DMF, UV exposure using fresh solutions for a total of 15 min; for photo-patterning functionalisation, IPA/water 1/1 v/v was used as the solvent instead (as DMF reacted with photomasks).

Thiol-ene reaction via micro-contact printing

Photoinitiated thiol-ene reactions via micro-contact printing were carried out according to a published procedure[39]. For each reaction, ethanol was deoxygenated via nitrogen gas bubbling for at least 15 min. A thiol solution was prepared by dissolving a thiol of interest (30 mM **T2** or **T5**, or 50 mM **T3**) and photoinitiator **P3** (15 mM for **T2** or **T5**, or 30 mM for **T3**) in deoxygenated ethanol (typical solvent used for transfer of molecules to PDMS stamps). A PDMS stamp was plasma-oxidised for a desired time (typically 15 s). A few drops of the thiol solution (20-30 µL) were transferred onto the stamp, left for ~1 min and the excess thiol solution was removed under a stream of nitrogen gas. The stamp was placed on a substrate (~1 × 1 cm^2) according to the set-up as illustrated in Figure S8 and irradiated with UV at 365 nm continuously for 15 min. The substrate was removed from the stamp and rinsed thoroughly with ethanol and water before drying under a stream of nitrogen gas. Flat PDMS stamps were used for homogeneous functionalisation. For reactive micro-contact printing patterning, two cycles of thiol solution incubation and drying were carried out after plasma-oxidisation for 2 s.

Generation of free PGMA via solution ATRP

A monomer solution containing GMA, bipy, Cu(ii)Br_2, Cu(i)Cl in methanol/water (4/1 v/v, 12 mL) was prepared according to the same procedure and formulation as in 'Generation of polymer brushes via surface-initiated ATRP'. Free ATRP initiator **2** (1.05 g, 2.2 mmol) was added to methanol/water (4/1 v/v, 3 mL) and the solution was degassed via nitrogen gas bubbling for 20 min with continuous stirring. The initiator solution was transferred to the monomer solution using a degassed syringe and ATRP was allowed to proceed with continuous stirring at RT for ~30 min until a large polymer lump was formed. The lump was removed and stirred in acetone to yield a blue/green polymer dispersion. Dilution of the dispersion using methanol produced a white dispersion and subsequent addition of THF generated a clear solution. The polymer solution was concentrated, precipitated in diethyl ether (DEE) and filtered (Whatman 1). Polymers were redissolved in THF and precipitated in DEE twice. Following this, polymers were redissolved in THF, passed through a flash column of silica gel (silica gel 60, 40-63 µm), precipitated in DEE, filtered and dried under high vacuum. This afforded ~3 g powder of free PGMA (f-PGMA) with a degree of polymerisation of 80 according to ^{1}H NMR.

Aminolysis of f-PGMA

Each sample was prepared by mixing a solution of f-PGMA (17 mg, ~120 µmol GMA repeat unit) in DMF (125 µL) with a solution containing allylamine (4 M), Et_3N (25 mol% with respect to allylamine) in DMF (125 µL). The reaction was allowed to proceed at 40 °C for 24 h. Polymers were subsequently precipitated in DEE, collected via vacuum filtration (Whatman 1) and dried under high vacuum for ATR-FTIR analysis. For NMR analysis, the polymers were dissolved in deuterated solvents immediately upon precipitation and filtration (as they became insoluble in any solvent upon drying under high vacuum).

Non-specific protein adsorption (BSA assay)

Coated glass substrates were placed in a 24-well cell culture plate and immersed in PBS (350 µL per substrate) for 15 min. A solution of BSA-dye in PBS (20 µg/mL, 350 µL) was added to each substrate, mixed thoroughly and incubated in the dark for 30 min on a shaker (150 rpm). The BSA-dye solution was diluted using PBS via serial dilution (2 mL per substrate, 5 series). After the final dilution, substrates were left in the solutions for 30 min on a shaker and protected from light. Care was taken to ensure substrates were submerged in solutions at all times. Each substrate was then washed using PBS via three cycles of solution aspiration/refilling (1 mL). Substrates were rinsed thoroughly with water and dried under a stream of nitrogen gas immediately before fluorescence microscopy.

Characterisation

The dry polymer thickness on silicon wafers was measured using an α-SE® spectroscopic ellipsometer (J. A. Woollam) at an incident angle of 70°. A silicon substrate/Cauchy film model was used and fitted between 400 nm and 900 nm. Transmission FTIR spectra were produced using a Bruker Tensor 27 spectrometer equipped with a MCT detector. Measurements were taken at 4 cm^{-1} resolution with 16 scans in the range of 600-4000 cm^{-1}, where the background measurement was conducted with a pure silicon wafer. ATR-FTIR spectra were acquired at a resolution of 4 cm^{-1} and a total of 128 scans per run (Perkin Elmer Spectrum 100). Static water contact angles were measured on a FTA1000 contact angle instrument (First Ten Ångstroms) at RT. For each measurement, a droplet of water (2 µL) was formed at a blunt-tip needle and brought into contact with a surface. Subsequently, the needle was retracted from the droplet, a series of 200 images were taken (5 images s^{-1}) and a mean contact angle was calculated. AFM was performed for dry samples on a Dimension 3100 microscope (Veeco Instruments) using the tapping mode. Olympus OMCL-AC series silicon probes with a resonant frequency of 300 kHz and a spring constant of 42 N m^{-1} were used. Images were acquired at a scan rate of 0.3-0.5 Hz for an area of 10 × 10 μm^2 and processed using the NanoScope software (Veeco Instruments).

XPS was carried out using a Kratos Axis Ultra DLD electron spectrometer with a monochromated Al Kα source (1486.6 eV) operated at 150 W. A pass energy of 160 eV and a step size of 1 eV were used for survey spectra. For high energy resolution spectra of regions, a pass energy of 20 eV and a step size of 0.1 eV were used. The spectrometer charge neutralising system was used to compensate sample charging and the binding scale was referenced to the aliphatic component of C 1s spectra at 285.0 eV. The concentrations obtained (error less than ± 10%) are reported as the percentage of that particular atom species (atomic %) at the surface of the sample (<10 nm analysis depth) without any correction. The analysis area (0.3×0.7 mm^2), the angle of incidence and the beam intensity were kept constant for all measurements. NMR spectroscopy was performed at 500 MHz (Bruker Avance 500 Cryo Ultrashield). Fluorescence microscopy was carried out for dry substrates on a Nikon Eclipse ME600 microscope. Fluorescence intensity was measured at three different positions on each substrate and the background (glass substrates coated with POEGMA brushes measured under the same exposure time) was subtracted. All background-corrected fluorescence intensities were normalised to 500 ms exposure time using a calibration curve (generated using APTMS-coated glass substrates; fluorescence intensities and a range of exposure times from 125 ms to 1 s exhibited a linear relationship with $R^2 \approx 0.9924$). The relative fluorescence intensity of substrates was calculated with respect to APTMS-coated glass substrates (internal reference) and the values are expressed as mean ± standard error. 2D profiles were generated via Image J software and plotted grey values against distance.

Results and discussion

Functionalisation of PGMA brushes with allylamine and propargylamine

Owing to the possibility of radical transfer to alkenes and alkynes during radical polymerisation, thiol-ene and thiol-yne reactive brushes were prepared in two stages. A PGMA brush was prepared first, via an ATRP process initiated from silicon substrates modified with a silane initiator[40]. This brush was selected due to the good control of its polymerisation over a wide range of thicknesses and inherent reactivity towards coupling with amines. Indeed, PGMA brush growth catalysed by a $CuCl/CuBr_2$/bipy ligand system in water/methanol 1/4 was found to proceed with a linear increase in thickness beyond 120 nm (Supplementary Figure S1). This is in good agreement with kinetics of PGMA brush growth previously reported in the literature[41].

In order to explore and quantify the amine functionalisation conditions, free PGMA polymers were reacted with allylamine and propargylamine in DMF. It was found that the functionalisation was complete after incubation in the amine solution for 24 h, in mild conditions (40 °C). Upon aminolysis in these conditions, ^{1}H NMR clearly showed the disappearance of the peaks corresponding to the protons adjacent to the epoxide, indicating full opening of the epoxide ring (Supplementary Figure S2). In addition, the appearance of allylic protons corresponding to a total of three protons compared to the protons of the main methacrylate backbone (ratio of 3.17 for protons g/b in Figure S2) confirmed that reaction with allylamine is quantitative. Similarly, the spectrum of free PGMA functionalised with propargylamine featured a proton (g in Figure S2) overlapping with the two protons adjacent to the amine (f) in the 1.7 to 2.1 ppm range. Considering the overlap of several peaks in the 2.4 to 3.7 ppm region of the spectrum, we used ^{13}C NMR to further confirm the presence of propargylic protons in free PGMA-pa, at 73.78 and 82.05 ppm. This was in good agreement with FTIR spectra (Supplementary Figure S3) showing the disappearance of the 906 cm^{-1} (anti-symmetric ring deformation of the epoxide group) and 850 cm^{-1} bands (symmetric ring deformation of the epoxide group)[38]. These bands were found to disappear upon aminolysis. In the case of functionalisation with allylamine, this was correlated with the appearance of a band at 920 cm^{-1} (trans =C–H wagging). Free PGMA-aa and PGMA-pa both displayed a broad absorption band ranging from 3100 cm^{-1} to 3700 cm^{-1}, characteristic of O–H and N–H stretching. In addition, these polymers displayed a band at 2835 cm^{-1} corresponding to C–H stretching next to amines. Hence our NMR and FTIR data were consistent with quantitative aminolysis of free PGMA polymers in these experimental conditions.

The aminolysis of PGMA brushes was investigated next. The change in dry brush thickness as a function of aminolysis time was monitored by ellipsometry and showed an increase in brush height over the first 14 h, followed by a plateau at longer incubation times (see Figure 1). The functionalisation level of the resulting PGMA-aa brushes was estimated from the change in ellipsometric thickness using equation S6 (see supplementary information). The functionalisation was found to plateau between 50 and 80 %, in contrast to the quantitative reactivity of free PGMA towards aminolysis. Similar results were obtained for the reaction of PGMA brushes with propargylamine (see Supplementary Figure S4) and confirmed by XPS measurements (Supplementary Figure S5 and Table 1). FTIR results also confirmed the functionalisation of PGMA brushes with amines, with the reduction of the bands at 850 and 906 cm^{-1} and the appearance of a broad band near 3300-3600 cm^{-1}, corresponding to O–H and N–H stretching vibrations, as well as the amine-associated C–H band at 2873 cm^{-1} (Figure 2). The functionalisation levels achieved are slightly higher than those reported for PGMA with small molecules amines in water, perhaps as a result of the better swelling of PGMA brushes in the solvent presently used (DMF), compared to water[38]. The increase in functionalisation level with increase in brush height is in good agreement with results obtained with poly(2-hydroxyethyl methacrylate) brushes, for which the functionalisation profile was found to be denser in the upper part of the brush and was strongly affected by the brush grafting density[42]. Such distribution of the functionalised groups is consistent with the dense crowding typical of polymer brushes that restrict molecular diffusion. Hence our

results suggest that thinner PGMA brushes are denser and do not allow full diffusion of amines, perhaps as a result of the decrease in chain density in the upper part of the brush[43, 44], as well as some level of termination in the initial stages of the polymerisation process[45].

Impact of initiating system on photo-activated thiol-ene coupling

The impact of the initiating system on photo-activated thiol-ene coupling to polymer brushes was first investigated as it was found to play an important role in the control of such reactions for the functionalisation of free polymer chains[24, 25]. The type of photoinitiator used to generate radicals was first investigated. Thermal initiators were not considered to avoid the degradation of polymer brushes and are not compatible with biomacromolecules and living cells that typically denature or die at such temperatures. Hence hydrogen abstraction (**P2** and **P3**, see Supplementary Scheme S1) and photo-cleavage type initiators (**P1** and **P4**) were considered. The irradiation time was varied between 0 and 15 min and the associated increase in brush thickness was monitored by ellipsometry, using cysteamine hydrochloride **T1** as a model thiol molecule. Coupling was found to occur predominantly between 3 and 5 min, with increases in dry brush thickness of 4 nm. This was mirrored by a rapid decrease in static water contact angles, which decreased by 15 to 25° over the same period of irradiation (see Figure 3). In the case of **T2** and **T4**, coupling was also evidenced by the band at 1640 cm^{-1} corresponding to amide I vibrations, in the FTIR spectra of the corresponding brushes (Figure 2). XPS also clearly indicated the occurrence of covalent coupling of thiols to brushes via the appearance of S 2p peaks in the region of 163-165 eV (see Figure 4). In addition, the increase in N 2p peaks and associated N atom content confirmed the functionalisation of PGMA-aa brushes with cysteamine. The functionalisation level calculated from XPS measurements is comparable to that derived from ellipsometry, although slightly lower, perhaps as a result of the hygroscopic properties of the resulting charged brushes (see Table 1). The rates of coupling for the different photoinitiators tested were very comparable, which contrast somewhat with reports suggesting that cleavage type initiators such as **P1** and **P4** are slightly more efficient to catalyse thiol-ene reactions[25]. This is perhaps the result of the large excess of thiol molecules used for surface functionalisation, compared to solution coupling of free polymers.

To confirm the selectivity and control of thiol-ene coupling to PGMA-aa brushes upon photo-activation, the reaction of cysteamine **T1** was carried out in the absence of photoinitiator, in the dark (no UV irradiation) and using a dark photomask (see Figure 5). In each case, the brush thickness remained unchanged throughout the experiment. This was confirmed by XPS (see Table 1), which showed no significant change in the atom composition compared to PGMA-aa. In addition, the water contact angle at the surface of the resulting brushes did not change substantially, although a slight decrease (5-10°) was observed (results not shown). However, when the reaction was carried out in the absence of thiol (so with photoinitiator and UV irradiation, but no thiol), the thickness of the brush increased. This phenomenon was observed for all photoinitiators tested (**P1-4**), but was stronger in the case of **P4** (see Figure 5). Such increase in brush thickness in the absence of thiol suggests that the photoinitiators are reacting with the alkene functions of PGMA-aa. This correlated with an absence of change in the XPS spectra of the resulting coatings, as the carbon and nitrogen contents measured remained unchanged (Table 1). In addition, in the case of PGMA-aa brushes reacted with **P4** in the absence of thiol, a phosphorus peak (P 2p) is observed by XPS (Supplementary Figure S5), confirming the coupling of the initiator to the brush. Hence, our data suggests that in the absence of thiol the radicals generated by photoinitiators **P1-4** can directly couple to alkene functionalised brushes. However, in the presence of thiol, transfer of the radical to the thiol molecules occurs much faster than direct coupling to the brush. This was confirmed by XPS, in the case of PGMA-aa reacted with **T1** in the presence of **P4**, as the resulting coating does not display any P 2p signal (Table 1).

The impact of ratio of thiol to photoinitiator and concentration of thiol was investigated next. This is an important aspect for biofunctionalisation considering the cost of even short peptide sequences and proteins. The ratio of acetyl cysteine **T2** to photoinitiator **P2** was varied from 100:1 to 1:10, with thiol concentrations ranging from 2500 to 2.5 mM (see Figure 5C). Decreasing the ratio of **T2** to **P2** from 100 to 10 was found to have relatively little effect on the functionalisation level, at high photoinitiator concentrations (25 mM), suggesting at such concentrations, sufficient levels of radicals are generated and transferred to thiols. When the photoinitiator concentration was decreased to 2.5, 0.25 and 0.15 mM, thiol coupling to brushes remained high (with functionalisation levels ranging from 55 to 33 %), providing the ratio of thiol to initiator was kept above 10. At lower ratios, the functionalisation level dropped significantly. Hence these results imply that efficient thiol-ene coupling requires a 10-fold excess of thiol and initiator concentrations above 150 μM, to ensure that thiyl radical concentrations are dominant and avoid scavenging and termination of the functionalisation process.

Similar coupling levels were achieved for the thiol-yne coupling of cysteamine **T1** to PGMA-pa brushes, with a functionalisation plateau reached around 5 min and 4 nm increase in dry brush thickness (using the photoinitiator **P1**, supplementary Figures S6 and S7). Such coupling was also specific to the presence of initiator and UV irradiation. However, considering that thiol-yne chemistry is potentially leading to bi-functionalisation of alkyne residues (with two thiol for each alkyne motif), the coupling levels are more modest than would be expected. This suggests that the crowding of PGMA-aa and PGMA-pa remains the most significant hurdle to their bio-functionalisation via thiol-ene and thiol-yne couplings. Potentially, higher coupling levels could be achieved at lower brush grafting densities.

Impact of thiol structure on coupling to brushes

Having investigated the role of thiol and photoinitiator concentrations and brush chemistry on the coupling of thiols, the impact of the chemical structure of the thiols to be coupled was investigated next. Thiol-ene coupling of a range of thiols (**T1-7**), with varying charge and size, on PGMA-aa brushes was studied via ellipsometry and XPS (results gathered in Table 1). The charge of the thiol was found to have strong impact on the efficiency of coupling to PGMA-aa brushes. Indeed, thiols **T2-4** have a negative charge and couple to higher levels (58-76%), compared to the positively charged **T1**. Given the presence of a secondary amine close to the alkene in the structure of PGMA-aa, this could suggest that some electrostatic repulsion occurs between the brush side chain and the thiols. However, this effect could also arise from the partial deprotonation of the thiol (into the corresponding thiolate) within the brush micro-environment, resulting in a loss of reactivity via thiol-ene. Both effects would be maximised due to the high brush grafting density typically achieved in the ATRP process[46]. These results are confirmed by XPS data obtained in comparable conditions and showing an increase in S 2p peak intensity in the case of **T2** and **T4** (Table 1, Figure 4 and supplementary Figure S5).

The size of the thiol was also found to have a marked impact on the coupling efficiency. Hence **T5-7**, with significantly higher molar masses (350 to 2,000 g/mol), couple with only 1-29% efficiency. This is not surprising considering the strong steric effect of these systems. Polymer-polymer coupling via thiol-ene is notoriously difficult to achieve and results in low conversions, even in the case of free polymers[47, 48]. It should also be pointed out that carbon-carbon recombinations and side reactions of the lower molecular weight fragments of the initiators with brushes are also expected to compete with the addition of thiyl radicals in the case of large thiols, consequently contributing to decreasing the overall coupling efficiency[48]. The steric penalty is even greater in the case of polymer brushes as their characteristic strong osmotic pressure prevent the diffusion of even moderately large molecules and therefore their reaction within the brush[49]. Therefore it is expected that moderately large molecules such as peptide sequences and small polymer chains would only functionalise the upper layer of polymer brushes. XPS (which typically only probes the first 5-10 nm of surfaces) provides some evidence for such hypothesis as the atomic composition determined for PGMA-aa-**T5** and -**T6** brushes accounts for functionalisation levels slightly higher than those determined by ellipsometry. This is in contrast with the lower functionalisation levels measured via XPS for thiols **T1-4**. The high grafting density of polymer brushes is therefore clearly detrimental to their reactivity with moderately large molecules, however this is not necessarily detrimental to the overall biofunctional properties of modified polymer brushes, since functional groups are often only required to be available in the upper compartment of the brush, for example for conferring cell adhesion or protein binding[12, 50].

Chemical patterning of brushes using thiol-ene chemistry

The ability to use photo-irradiation to activate thiol-ene coupling was used to control the chemical patterning of polymer brushes. Two different strategies were explored (see Supplementary Figure S8): the direct photolithography through a photomask and the use of a PDMS stamp combined with photo-irradiation for reactive micro-contact printing[51]. The direct photo-lithography approach is interesting as it does not require the generation of a master or stamp and avoids the direct mechanical contact with the brush. Acetate masks were used to sandwich a thin layer of thiol **T4** solution (10 μL drop) containing photoinitiator **P2** in contact with the brush. After 15 min photo-irradiation, the resulting patterns were examined via microscopy, the contrast of the patterned image resulting from the change in brush height (Figure 6). At first glance, the resulting patterns, whether 20 or 50 μm diameter discs, appear homogeneous and sharp with defined edges. Imaging of these patterns via AFM confirmed the increase in height of the brush by 20 nm, consistent with increases in brush thickness measured for this thiol via ellipsometry (25 nm increase, from a 30 nm PGMA-aa brush, corresponding to c.a. 74% functionalisation, in agreement with results from Table 1 determined via ellipsometry for **T4**). However, the edge of the pattern clearly appears graded, with a slope of 2 nm/μm. This is reasonable considering the mask was not in direct contact with the brush but had to be positioned slightly above to allow room for the thiol solution.

To improve the contour edge, the use of reactive micro-contact printing was investigated as this should prevent molecular diffusion and restrict chemical functionalisation to the contact area. To confirm the ability to carry out reactive micro-contact printing via thiol-ene coupling, we placed homogeneous (non-patterned) PDMS stamps, inked with thiol **T2** and photoinitiator **P1**, in contact with polymer brushes and measured the increase in brush thickness following to photo-irradiation via ellipsometry. For irradiation times ranging from 5 to 15 min, increases in brush height ranging from 8 to 11 nm were measured, whereas carrying out the same procedure without any photo-irradiation led to only 1-2 nm increase in brush height. Similarly, coupling of thiol **T3** gave rise to 8 nm increase in brush thickness, which compares well to the changes in brush thickness measured from solution coupling. Interestingly, the PEG thiol **T5** was found to couple to a higher level than in solution, with 32 nm increase in brush height, equivalent to 77% functionalisation level, suggesting that this thiol-ene reaction is more efficient when carried out in dry conditions, as in reactive micro-contact printing. Hence, overall these results confirm that the efficiency of thiol-ene based on photo-reactive micro-contact printing is comparable to that of thiol-ene coupling from solution.

Patterning of PGMA-aa brushes via thiol-ene photo-reactive micro-contact printing (with thiol **T2**) resulted in clear and reproducible patterns that matched the size of the original stamps (see Figure 7). In addition, when the resulting surfaces were exposed to water vapours, clear condensation patterns were observed, confirming the change in hydrophilicity of the surface (Figure 7). AFM characterisation of patterns obtained from **T2** clearly demonstrated the resolution that reactive

micro-contact printing confers, with sharp edges and contours of the printed features (10 nm/μm slope at the edge). Therefore, these results suggest that reactive micro-contact printing is an attractive technique to achieve high resolution patterning of polymer brushes via thiol-ene coupling. However, this approach is not always compatible with experimental conditions and direct photo-activated thiol-ene coupling is more suitable for *in situ* writing or functionalisation of polymer brushes, for example for the design of substrates able to stimulate cell adhesion and motility upon trigger[33].

Generation of protein patterns

The ability to modify and pattern the chemistry of polymer brushes is also attractive for protein patterning, whether for the design of sensing platforms[52, 53] or the generation of cellular patterns for the development of cell-based assays[7, 8, 54]. To demonstrate the feasibility of using thiol-ene chemistry for controlling protein adsorption and patterning to polymer brushes, the adsorption of bovine serum albumin (BSA) to PGMA-aa brushes before and after thiol-ene coupling was explored (see Figure 8). Compared to unfunctionalised poly(oligo ethylene glycol) methacrylate (POEGMA) brushes, BSA adsorption to PGMA-aa was strong, as judged by the intensity of fluorescence images taken for brush-coated samples immersed in a 20 μg/mL BSA solution. POEGMA is a particularly protein resistant coating, with no BSA absorption detected via surface plasmon resonance, even at moderately high concentrations (up to 1 mg/mL)[7], and hence provides a suitable negative control for this experiment. The high protein adsorption observed for PGMA-aa is consistent with the positive charge present in the structure of this brush, as for other cationic brushes which promote high protein adsorption, equivalent to the adsorption of multiple layers of proteins[54, 55]. Upon functionalisation with thiol **T3** and, the level of BSA adsorption decreased 3.4 fold (Figure 8), but was not fully suppressed, despite the neutralisation of the brush structure, perhaps owing to the only partial functionalisation of allylamine residues. Functionalisation with PEG thiol **T5** resulted in a further decrease in the adsorption level of BSA, especially when this coupling was carried out via reactive micro-contact printing, in agreement with the higher functionalisation level achieved via this approach. Hence the strong crowding induced by functionalisation with PEG thiol **T5** was sufficient to prevent diffusion and adhesion to the underlying positively charged compartments of the brush. This contrast between protein adsorption to PGMA-aa or PGMA-aa-**T2** brushes was used for the generation of BSA patterns (Figure 8). PGMA-aa brushes were photo-patterned using **T2**, followed by passivation of the background with PEG thiol **T5**. When passivation was omitted, the level of background remained relatively high. However, when **T5** coupling was carried out via reactive micro-contact printing, the background decreased significantly, resulting in well-defined protein islands with a dark background (Figure 8C and E).

Conclusions

Thiol-ene coupling is a remarkably efficient reaction for biofunctionalisation of biomaterials, due to the possibility to engineer in cysteine residues in peptides, at sufficiently low level for controlling the coupling orientation, and the absence of carbon-carbon double bonds from these molecules. This coupling was found to be a robust option for the biofunctionalisation of polymer brushes, even in the case of relatively protein resistant brushes, although its efficiency decreases markedly as the molecular weight of the thiol-bearing molecules increases. The density of brushes was found to confine functionalisation to the surface of brushes, presumably as a result of restricted molecular diffusion. In addition, it was found that thiol-ene chemistry is very well suited for photo-patterning of bioactive molecules, a useful feature for the structuring of biomaterials and the control of cell behaviour. The work presented here is expected to also allow the anchorage of proteins bearing free cysteines. Hence thiol-ene coupling is a particularly useful method for the biofunctionalisation of tissue culture platforms and implants, for regenerative medicine, as well as the decoration of biosensors with sensing molecules. It offers opportunities to orientate bioactive molecules at the surface of non-fouling polymer coatings. Some challenges remain to allow wide-spread use of such coupling in the biomedical field, for example the control of thiol-ene chemistry at low thiol concentration or in physiological conditions, and its activation with low toxicity initiators requiring visible light irradiation rather than UV-light.

Acknowledgements

Funding from the Royal Society (RG110425), the Swedish Research Council (Grant 621-2011-3504) and the Swedish Foundation for International Cooperation in Research and Higher Education (Grant IG2011-2048) are acknowledged. K.Y.T. thanks Schlumberger for funding.

References

1 I. Banerjee, R. C. Pangule and R. S. Kane, *Adv. Mater.*, 2011, **23**, 690-718.
2 S. Jiang and Z. Cao, *Adv. Mater.*, 2010, **22**, 920-932.
3 J. E. Raynor, J. R. Capadona, D. M. Collard, T. A. Petrie and A. Garcia, *Biointerphases*, 2009, **4**, 3-16.
4 M. Krishnamoorthy, S. Hakobyan, M. Ramstedt and J. E. Gautrot, *Chem. Rev.*, 2014, **114**, 10976-11026.
5 R. Barbey, L. Lavanant, D. Paripovic, N. Schuwer, C. Sugnaux, S. Tugulu and H.-A. Klok, *Chem. Rev.*, 2009, **109**, 5437-5527.
6 O. Azzaroni, *J. Polym. Sci., A: Polym. Chem.*, 2012, **50**, 3225-3258.
7 J. E. Gautrot, B. Trappmann, F. Oceguera-Yanez, J. Connelly, X. He, F. M. Watt and W. T. S. Huck, *Biomaterials*, 2010, **31**, 5030-5041.
8 J. E. Gautrot, C. Wang, X. Liu, S. J. Goldie, B. Trappmann, W. T. S. Huck and F. M. Watt, *Biomaterials, 2012*, **33**, 5221-5229.
9 J. E. Gautrot, J. Malmstrom, M. Sundh, C. Margadant, A. Sonnenberg and D. S. Sutherland, *Nano Lett.*, 2014, **14**, 3945-3952.

10 J. Connelly, J. E. Gautrot, B. Trappmann, D. W. M. Tan, G. Donati, W. T. S. Huck and F. M. Watt, *Nat. Cell Biol.*, 2010, **12**, 711-718.
11 H. Jiang and F.-J. Xu, *Chem. Soc. Rev.*, 2013, **42**, 3394-3426.
12 J. Trmcic-Cvita, E. Hasan, M. Ramstedt, X. Li, M. Cooper, C. Abel, W. T. S. Huck and J. E. Gautrot, *Biomacromolecules*, 2009, **10**, 2885-2894.
13 H. Vaisocherova, W. Yang, Z. Zhang, Z. Cao, G. Cheng, M. Piliarik, J. Homola and S. Jiang, *Anal. Chem.*, 2008, **80**, 7894-7901.
14 S. Tugulu, P. Silacci, N. Stergiopulos and H.-A. Klok, *Biomaterials*, 2007, **28**, 2536-2546.
15 K. Glinel, A. M. Jonas, T. Jouenne, J. Leprince, L. Galas and W. T. S. Huck, *Bioconj. Chem.*, 2009, **20**, 71-77.
16 J. Sha, E. S. Lippmann, J. McNulty, Y. Ma and R. S. Ashton, *Biomacromolecules*, 2013, **14**, 3294-3303.
17 P. Jain, L. Sun, J. Dai, G. L. Baker and M. Bruening, *Biomacromolecules*, 2007, **8**, 3102-3107.
18 J. E. Gautrot, W. T. S. Huck, M. Welch and M. Ramstedt, *Appl. Mater. Interfaces*, 2010, **51**, 193-202.
19 S. V. Orski, A. A. Poloukhtine, S. Arumugam, L. Mao, V. V. Popik and J. Locklin, *J. Am. Chem. Soc.*, 2010, **132**, 11024-11026.
20 A. R. Kuzmyn, A. de los Santos Pereira, O. Pop-Georgievski, M. Bruns, E. Brynda and C. Rodriguez-Emmenegger, *Polym. Chem.*, 2014, **5**, 4124-4131.
21 A. de los Santos Pereira, N. Y. Kostina, M. Bruns, C. Rodriguez-Emmenegger and C. Barner-Kowollik, *Langmuir*, 2015, **31**, 5899-5907.
22 C. E. Hoyle, T. Y. Lee and T. Roper, *J. Polym. Sci., A: Polym. Chem.*, 2004, **42**, 5301-5338.
23 A. Dondoni, *Angew. Chem., Int. Ed.*, 2008, **47**, 8995-8997.
24 L. M. Campos, K. L. Killops, R. Sakai, J. M. J. Paulusse, D. Damiron, E. Drockenmuller, B. W. Messmore and C. J. Hawker, *Macromolecules*, 2008, **41**, 7063-7070.
25 M. Uygun, M. A. Tasdelen and Y. Yagci, *Macromol. Chem. Phys.*, 2010, **211**, 103-110.
26 R. M. Hensarling, V. A. Doughty, J. W. Chan and D. L. Patton, *J. Am. Chem. Soc.*, 2009, **131**, 14673-14675.
27 J. Mergy, A. Fournier, E. Hachet and R. Auzely-Velty, *J. Polym. Sci., A: Polym. Chem.*, 2012, **50**, 4019-4028.
28 Y. Fu, K. Xu, X. Zheng, A. J. Giacomin, A. W. Mix and W. J. Kao, *Biomaterials*, 2012, **33**, 48-58.
29 N. Gupta, B. F. Lin, L. M. Campos, M. D. Dimitriou, S. T. Hikita, N. D. Treat, M. V. Tirrell, D. O. Clegg, E. J. Kramer and C. J. Hawker, *Nat. Chem.*, 2010, 138-145.
30 P. Jonkheijm, D. Weinrich, M. Kohn, H. Engelkamp, P. C. M. Christianen, J. Khuhlmann, J. C. Maan, D. Nusse, H. Schroeder, R. Wacker, R. Breinbauer, C. M. Niemeyer and H. Waldmann, *Angew. Chem., Int. Ed.*, 2008, **47**, 4421-4424.
31 M. Dubner, T. N. Gevrek, A. Sanyal, N. D. Spencer and C. Padeste, *Appl. Mater. Interfaces*, 2015, **7**, 11337-11345.
32 M. Khan, J. Yang, C. Shi, J. Lv, Y. Feng and W. Zhang, *Acta Biomater*, 2015, **20**, 69-81.
33 P. Costa, J. E. Gautrot and J. Connelly, *Acta Biomater*, 2014, 10.1016/j.actbio.2014.1001.1029.
34 X.-S. Wang and S. P. Armes, *Macromolecules*, 2000, **33**, 6640-6647.
35 D. Qin, Y. Xia and G. M. Whitesides, *Nat. Protoc.*, 2010, **5**, 491-502.
36 K. Y. Tan, J. E. Gautrot and W. T. S. Huck, *Langmuir*, 2011, **27**, 1251-1259.
37 S. Edmondson and W. T. S. Huck, *J. Mater. Chem.*, 2004, **14**, 730.
38 R. Barbey and H.-A. Klok, *Langmuir*, 2010, **26**, 18219-18230.
39 C. Wendeln, S. Rinnen, C. Schulz, H. F. Arlinghaus and B. J. Ravoo, *Langmuir*, 2010, **26**, 15966-15971.
40 A. M. Jonas, K. Glinel, R. Oren, B. Nysten and W. T. S. Huck, *Macromolecules*, 2007, **40**, 4403-4405.
41 S. Edmondson and W. T. S. Huck, *J. Mat. Chem.*, 2004, **14**, 730-734.
42 N. Schuwer, T. Geue, J. P. Hinestrosa and H.-A. Klok, *Macromolecules*, 2011, **44**, 6868-6874.
43 I. G. Elliott, T. L. Kuhl and R. Faller, *Macromolecules*, 2010, **43**, 9131-9138.
44 S. T. Milner, T. A. Witten and M. E. Cates, *Macromolecules*, 1989, **22**, 853-861.
45 N. Cheng, O. Azzaroni, S. Moya and W. T. S. Huck, *Macromol. Rapid Commun.*, 2006, **27**, 1632-1636.
46 D. M. Jones, A. A. Brown and W. T. S. Huck, *Langmuir*, 2002, **18**, 1265-1269.
47 S. P. S. Koo, M. M. Stamenovic, R. A. Prasath, A. J. Inglis, F. E. Du Prez, C. Barner-Kowollik, W. Van Camp and T. Junkers, *J. Polym. Sci., A: Polym. Chem.*, 2010, **48**, 1699-1713.
48 P. Derboven, D. R. D'hooge, M. M. Stamenovic, P. Espeel, G. B. Marin, F. E. Du Prez and M.-F. Reyniers, *Macromolecules*, 2013, **46**, 1732-1742.
49 H.-S. Lee and L. S. Penn, *Langmuir*, 2009, **25**, 7983-7989.
50 M. Navarro, E. M. Benetti, S. Zapotoczny, J. A. Planell and G. J. Vancso, *Langmuir*, 2008, **24**, 10996-11002.
51 J. Lahiri, E. Ostuni and G. M. Whitesides, *Langmuir*, 1999, **15**, 2055-2060.
52 A. Hucknall, D.-H. Kim, S. Rangarajan, R. T. Hill, W. M. Reichert and A. Chilkoti, *Adv. Mater.*, 2009, **21**, 1968-1971.
53 R. Barbey, E. Kauffmann, M. Ehrat and H.-A. Klok, *Biomacromolecules*, 2010, **11**, 3467-3479.
54 K. Y. Tan, H. Lin, M. Ramstedt, F. M. Watt, W. T. S. Huck and J. E. Gautrot, *Integr. Biol.*, 2013, **5**, 899-910.
55 A. Wittemann and M. Ballauff, *Phys. Chem. Chem. Phys.*, 2006, **8**, 5269-5275.

Polymer Chemistry

ARTICLE

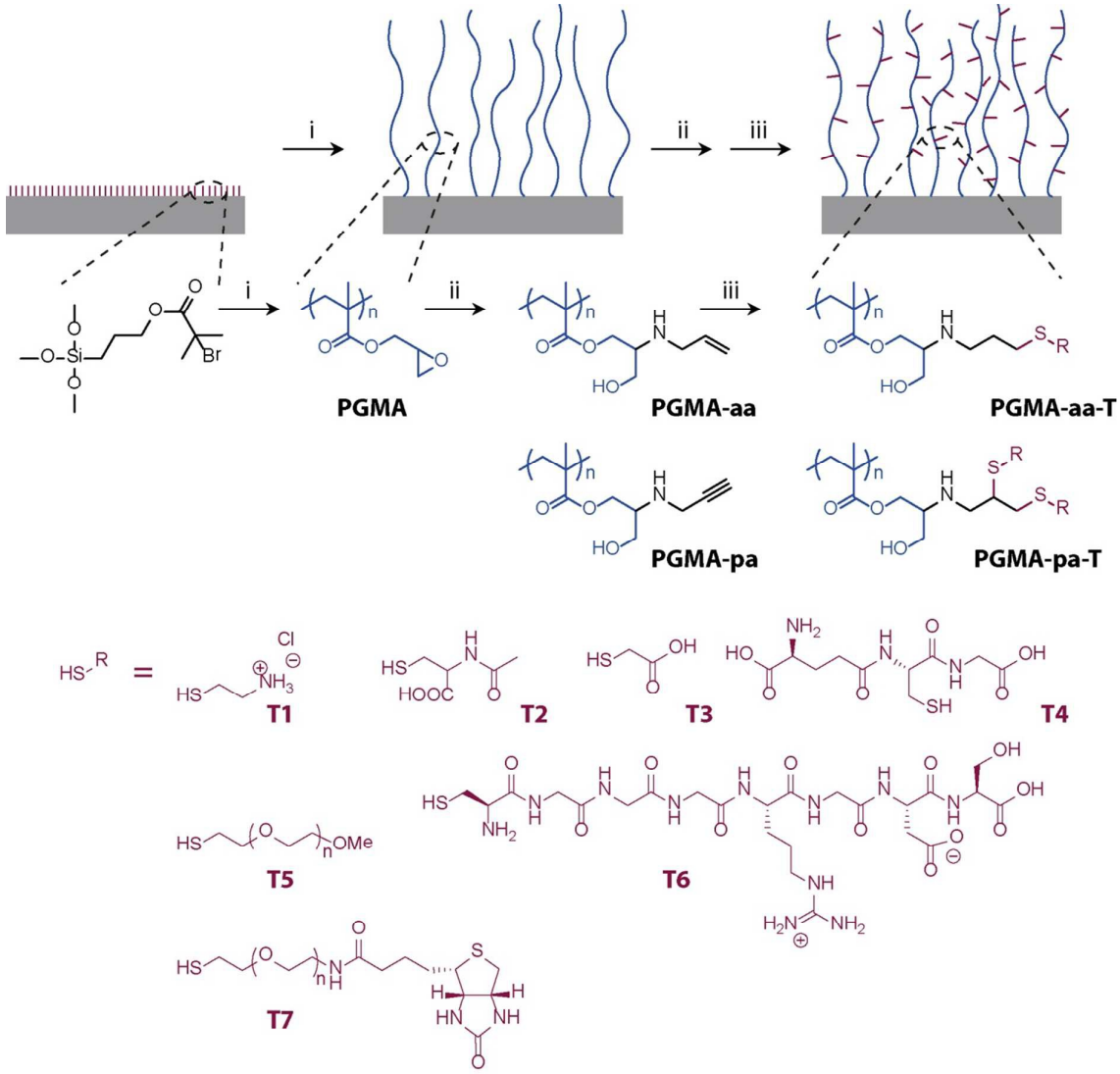

Scheme 1. PGMA brush growth and functionalisation via thiol-ene and thiol-yne chemistry.

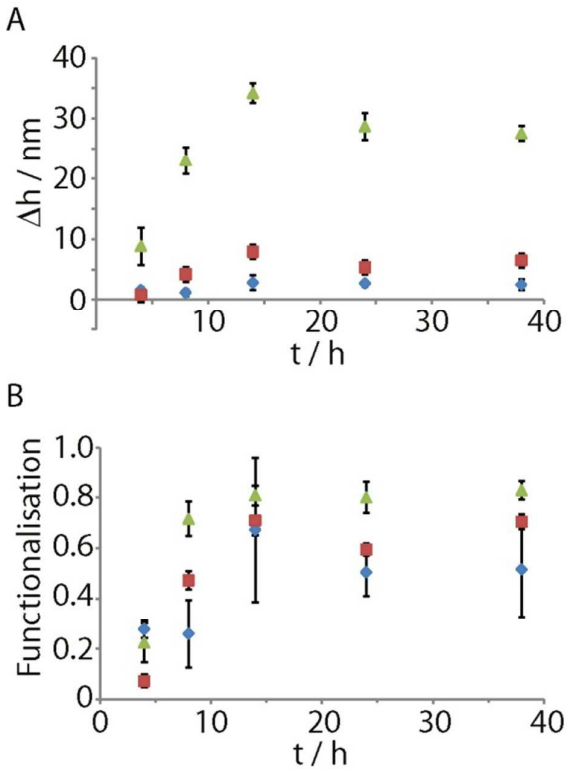

Figure 1. Functionalisation of PGMA brushes with allylamine. A, changes in dry brush thickness measured by ellipsometry. B, corresponding functionalisation levels. Starting PGMA brush thicknesses were: 12 nm, blue diamonds, 25 nm, red squares, 91 nm, green triangles.

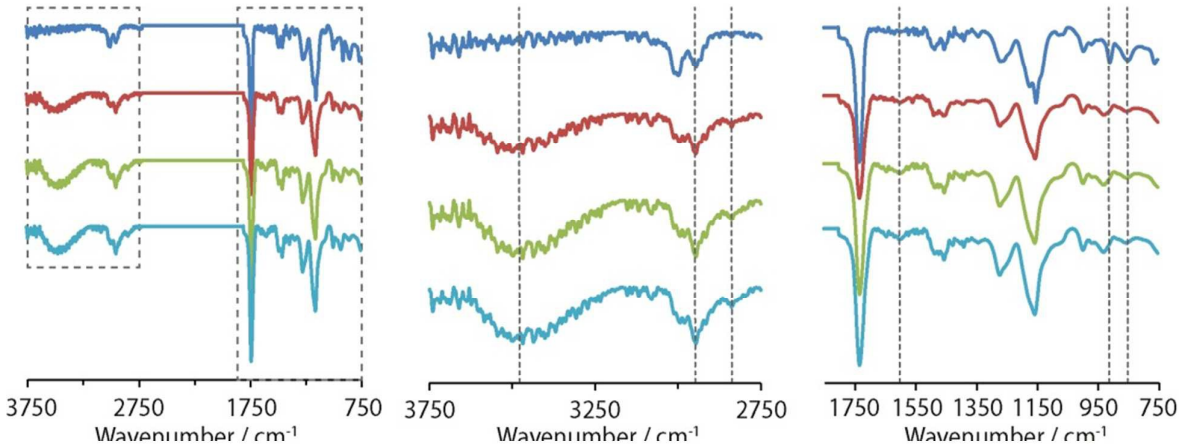

Figure 2. FTIR of functionalised PGMA brushes. From top to bottom: PGMA brush, before (dark blue) and after (red) allylamine functionalisation, and PGMA-aa-**T2** (green) and PGMA-aa-**T4** (light blue) using the photoinitiator **P2**.

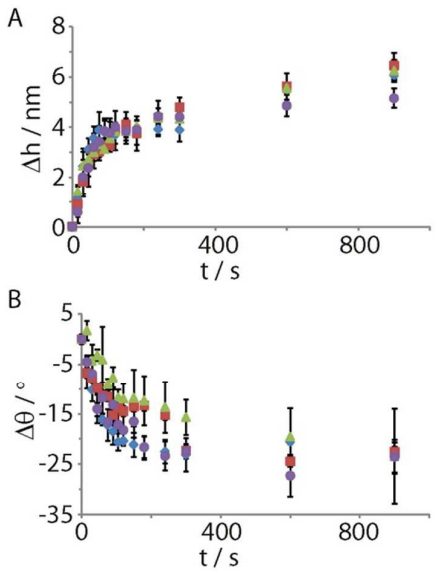

Figure 3. Thiol-ene reaction on PGMA-aa brushes. Increase in brush thickness (A) and change in contact angle (B) during the reaction of PGMA-aa with **T1** and **P1-4** (2 wt%; P1, blue diamonds; P2, red squares; P3, green triangles; P4, purple circles).

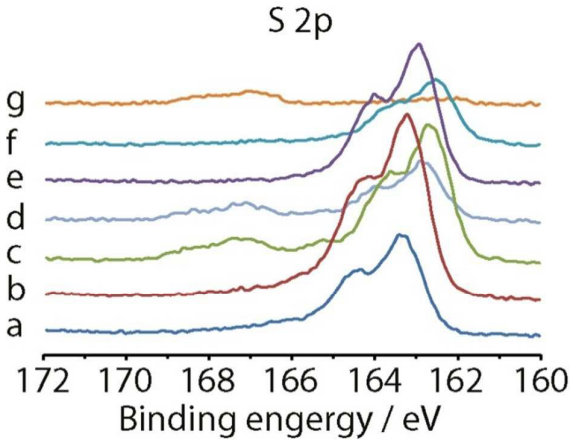

Figure 4. XPS spectra (S 2p) for: a, PGMA-aa-**T1**, b, PGMA-aa-**T1** (with **P4**), c, PGMA-aa-**T2**, d, PGMA-aa-**T3** (with **P1**), e, PGMA-aa-**T4**, f, PGMA-aa-**T5**, g, PGMA-aa-**T6**. Thiol-ene reactions were carried using photoinitiator **P2**, unless otherwise stated.

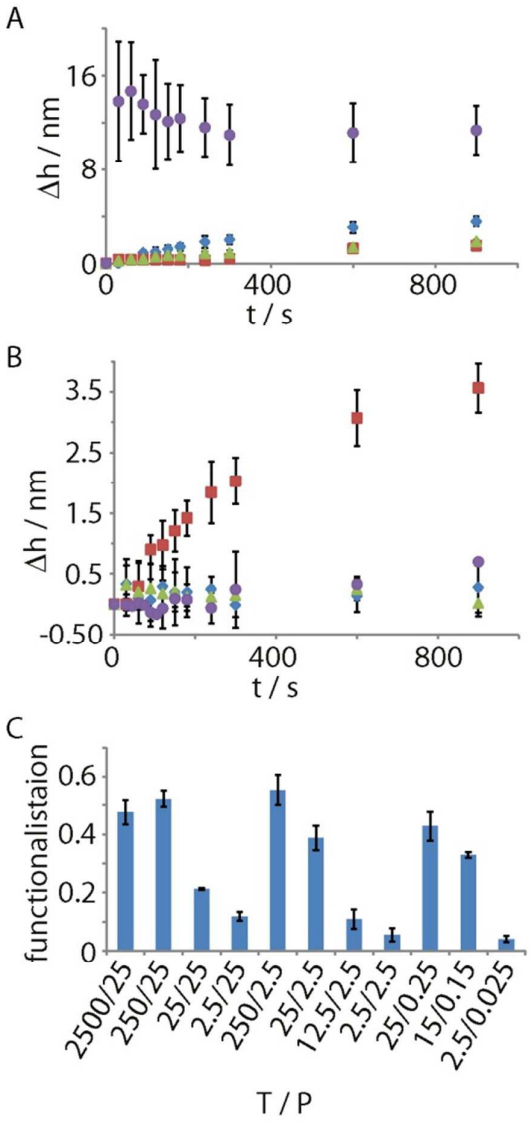

Figure 5. Impact of thiol-ene reaction conditions on coupling. A, reaction with **P1** (blue diamond), **P2** (red squares), **P3** (green triangles) and **P4** (purple circles) in the absence of thiol, monitored by ellipsometry. B, reaction of PGMA-aa without **T1** (red squares), **P1** (blue diamonds), UV (green triangles) or with a dark photomask (purple circles). Δh are the changes in ellipsometric thickness measured with respect to the starting PGMA-aa brushes. C, impact of ratio **T2/P2** on the functionalisation level, measured by ellipsometry, of PGMA-aa with acetyl cysteine **T2** under 15 min of UV irradiation in the presence of photoinitiator **P2**.

Polymer Chemistry

ARTICLE

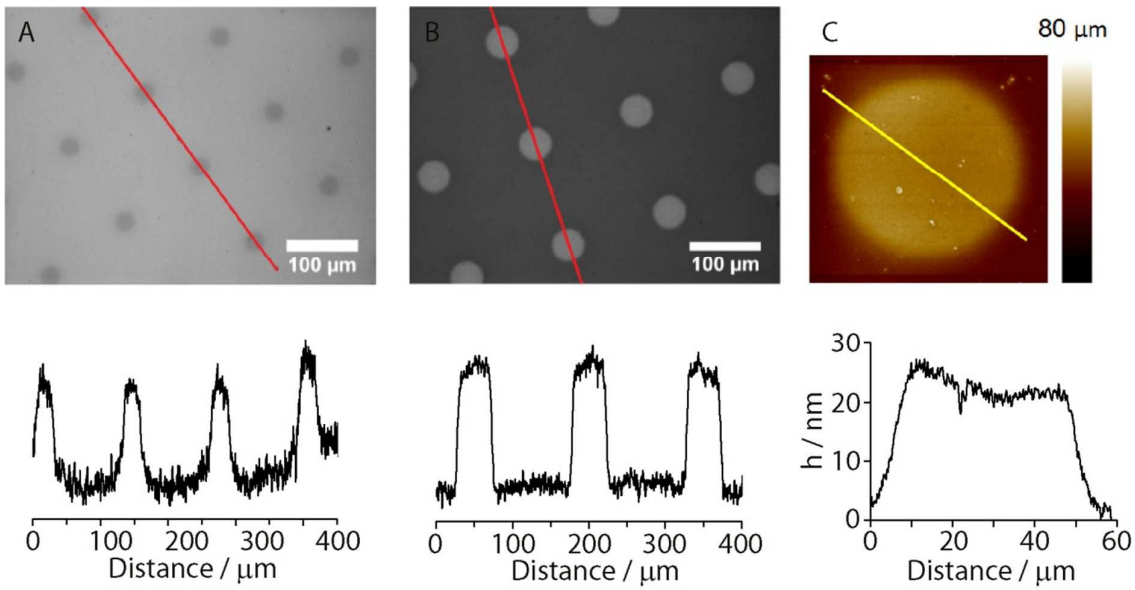

Figure 6. Photo-patterning of polymer brushes using thiol-ene chemistry. A. Photo-patterning of **T4** islands (30 µm) on PGMA-aa brushes (25 mM **T4**, 2.5 mM **P2**, 15 min UV irradiation). Top, microscopy image; bottom, corresponding intensity profile (inverted). B. Photo-patterning of **T4** in identical conditions as A, with 50 µm islands. Top, microscopy image; bottom, corresponding intensity profile. C. AFM image of a 50 µm island functionalised with **T4**. Top, AFM image in tapping mode; bottom, corresponding profile. Initial thickness of PGMA-aa brushes: A and B, 70 ± 2.6 nm.

Polymer Chemistry

ARTICLE

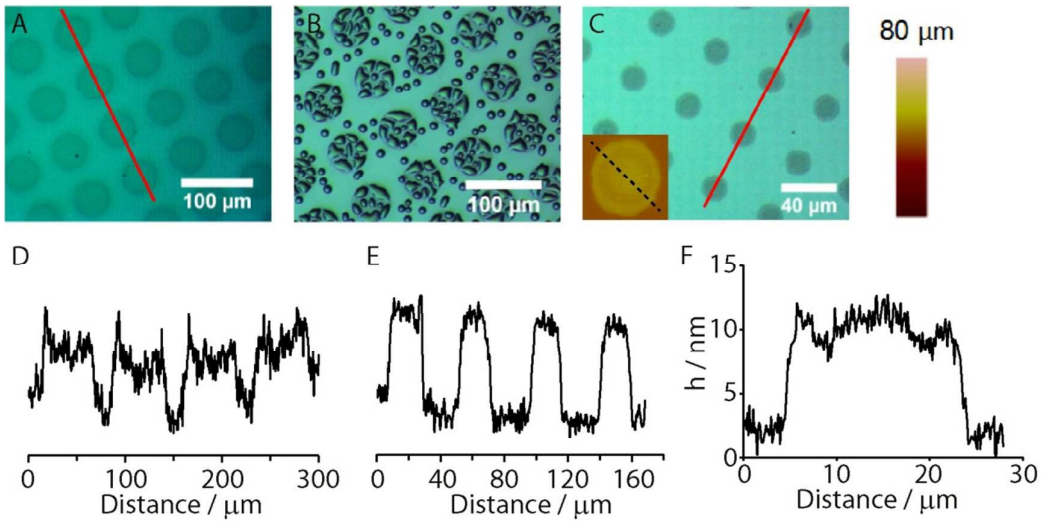

Figure 7. Photo-activated micro-contact printing on polymer brushes. A. Microscopy image of 50 µm islands generated by reactive micro-contact printing of **T2** on PGMA-aa. B. Corresponding condensation pattern (after short exposure to water vapours). C. Microscopy image of 20 µm islands generated by reactive micro-contact printing of **T2** on PGMA-aa. The inset is an AFM image (22 by 22 µm) of one of these islands. D. Intensity profile corresponding to the red line drawn in A. E. Intensity profile corresponding to the red line drawn in C. F. Height profile along the dashed line in the inset of C. Initial thickness of PGMA-aa brushes: A, 26 ± 0.2 nm. C, 50 ± 1.6 nm.

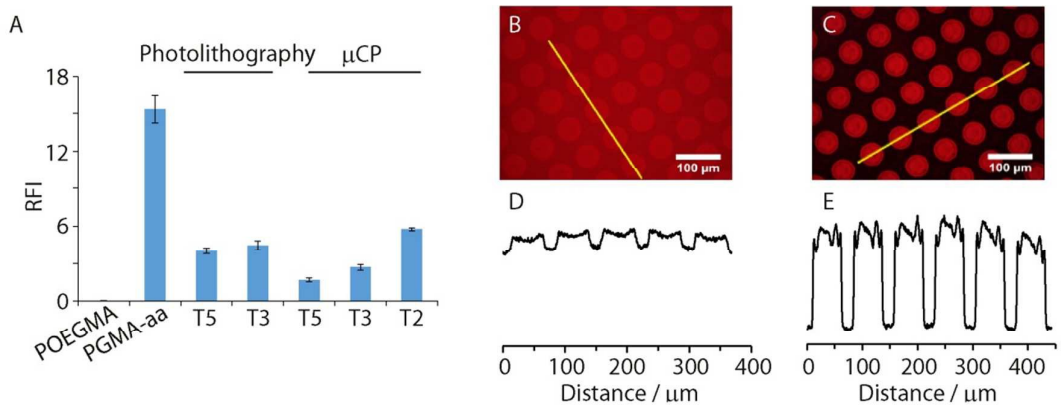

Figure 8. Protein patterning on thiol-ene patterned polymer brushes via photo-activated micro-contact printing. A. protein adsorption (BSA) to PGMA-aa brushes before and after functionalisation with different thiols. POEGMA is used as negative control. RFI is the relative fluorescence intensity compared to APTMS-coated glass. B and C. Fluorescence microscopy image of BSA patterns generated using patterned PGMA-aa-**T2** without (B) and with (C) protection of the background with **T5** (via reactive micro-contact printing with a flat PDMS stamp). D and E are the intensity profiles corresponding to images B and C respectively.

Polymer Chemistry

ARTICLE

Table 1. XPS and ellipsometric characterisation of thiol-ene reacted polymer brushes reported as percentage atomic concentration of the surface. f1 and f2, functionalisation levels of aminolysis and thiol-ene coupling respectively determined via ellipsometry (± standard deviation); f3, functionalisation level of thiol-ene coupling determined via XPS (± experimental error). Calculations of the functionalisation levels are given in supplementary information.

	Conditions	Initial thickness (nm)	Post-functionalisation thickness (nm)	O	C	N	S	P	Si	f1 or f2 (%)	f3 (%)
PGMA		19.0±0.3		23.6	76.4						
PGMA-aa		19.7±0.4	24.4±0.6	18.5	75.7	5.8				60±12	77±15
PGMA-pa		19.1±0.3	23.2±0.0	20.5	73.5	4.7			1.3	56±4	64±13
PGMA-aa-T1	**P2**	24.5±0.3	28.0±0.4	16.8	74.5	6.8	1.9			37±7	31±6
PGMA-aa-T1	**P4**	24.4±0.1	29.7±0.1	15.1	73.5	7.8	3.5				57±12
PGMA-aa	**P2**, **T1**, no UV	25.5±0.1	25.5±0.1	18.3	75.8	6.0					
PGMA-aa	**T1**, no photoinitiator	23.8±0.2	24.0±0.1	18.1	76.1	5.8					
PGMA-aa	**P2**, no thiol	24.2±0.1	24.6±0.1	18.9	75.6	5.6					
PGMA-aa	**P4**, no thiol	24.0±0.2	31.0±0.5	18.6	74.9	4.5		2.0			
PGMA-aa-T2	**P2**	25.1±0.3	35.4±0.4	20.6	69.8	6.8	2.8			76±6	60±12
PGMA-aa-T3	**P2**	26.1±0.5	30.5±1.8							58±30	
PGMA-aa-T3	µCP, **P1**	35.0±0.3	41.4±0.1	22.2	71.2	5.1	1.4				24±5
PGMA-aa-T4	**P2**	24.7±0.2	42.4±0.1	20.8	67.2	9.9	2.2			70±1	65±13
PGMA-aa-T5	**P2**	24.0±0.2	32.6±0.2	21.2	73.3	4.4	1.1			29±1	38 ±8
PGMA-aa-T6	**P2**	23.0±0.1	26.3±0.1	19.0	73.0	6.1	0.3		1.2	6±1	14±3
PGMA-aa-T7	**P2**	23.5±0.2	24.4±0.3							1±1	
PGMA-aa-T7	**P4**	25.4±0.0	33.3±0.3							5±1	

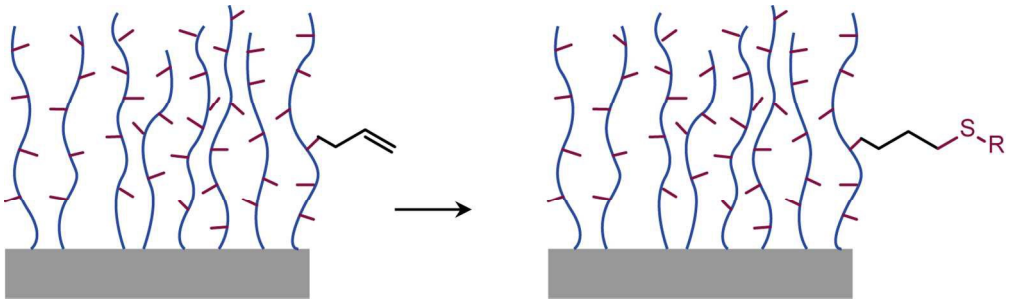

130x38mm (300 x 300 DPI)